

Selective ethylene oligomerisation using supported tungsten mono-imido catalysts

Christopher M. R. Wright, Thomas J. Williams, Zoë R. Turner, Jean-Charles Buffet and Dermot O'Hare*

Received 00th January 20xx,
Accepted 00th January 20xx

DOI: 10.1039/x0xx00000x

www.rsc.org/

A series of substituted phenyl mono-imido complexes of the type $W(NR)Cl_4(THF)$ ($R = C_6H_5$, 2,6-Me- C_6H_3 , 3,5-Me- C_6H_3 , 2,4,6-Me- C_6H_2 , 4-OMe- C_6H_4 , 2,6-F- C_6H_3 and 3,5-CF₃- C_6H_3) have been synthesised and characterised. Reaction of these complexes with solid polymethylaluminoxane (sMAO) leads to immobilisation and *in situ* methylation of the chloride positions on the surface of the support. Reaction of $W(NR)Cl_4(THF)$ with trimethylaluminium (TMA) yields the trimethyl complexes $W(NR)Me_3Cl$. Immobilisation of the isotopically labelled $W\{N(2,6-F-C_6H_3)\}(^{13}CH_3)_3Cl$ on sMAO furnished the supported complex with two identifiable methyl resonances in the $^{13}C\{^1H\}$ solid state CPMAS spectrum (45 and 56 ppm), with the latter matching the unsupported complex, confirming retention of the structure on the surface. The sMAO-supported complexes ($W:Al = 1:150$) were tested for their propensity to dimerise ethylene (1 bar) in *d*₆-benzene at 100 °C and compared with the previously reported sMAO- $W\{N(2,6-^iPr-C_6H_3)\}Cl_4(THF)$ (sMAO-1.a). Complexes with electron deficient imido groups were shown to be the most active, and increased steric bulk in the ortho positions is also an important factor, with sMAO acting as a support, scavenger and activator. sMAO- $W\{N(3,5-CF_3-C_6H_3)\}Cl_4(THF)$ was the most active, demonstrating a turnover frequency of 5.65 mol_{C₂H₄}mol⁻¹_Wh⁻¹ and a selectivity towards 1-butene of 91% after 8 h.

Introduction

Since the discovery of the monomeric group 6 imido complex $W(CHCMe_3)\{N(C_6H_5)\}(PEt_3)_2Cl_2$ in 1982,¹ tungsten *aryl* imido complexes have attracted significant interest especially in the area of olefin metathesis.^{2–4} Despite their role as spectator ligands, variation of the electronic and steric properties of the imido moiety can greatly affect the activity and stability of the catalysts. Hoveyda and co-workers have shown that modification of the imido fragment to be more electron deficient and less sterically encumbered, in complexes of the type $W(NAr)(CHCMe_3)(ODBMP)_2$ (DBMP = 2,6-CHPh₂-4-Me- C_6H_2), led to much higher rates of polymerisation of 2,3-dicarbomethoxynorbornadiene.⁵

In 1975, Menapace *et al.* reported that the selectivity of a metathesis catalyst comprised of WCl_6 , $PhNH_2$ and $Et_3Al_2Cl_3$ could be modified in favour of alkene dimerisation by increasing the amount of aluminium cocatalyst in the system.⁶ Furthermore, addition of triethylamine into the system with $EtAlCl_2$ as the cocatalyst resulted in selectivities >99% for the

dimerisation of 1-hexene.⁷ The active species in these ill-defined systems has been proposed to be a tungsten imido complex formed *in situ*. Independently, activation of both tungsten mono- and bis-imido (Chart 1, **A**) complexes with aluminium co-catalysts has yielded catalysts active for the dimerisation of olefins.^{8,9} In the mono-imido case however, no characterisation of the active species was performed. Recently, we reported that the well-defined tungsten mono-imido complex $W\{N[2,6-^iPr-C_6H_3]\}Me_3Cl$ (Chart 1, **2.a**), formed from the reaction of $W\{N[2,6-^iPr-C_6H_3]\}Cl_4(THF)$ (**1.a**) and $AlMe_3$, is active for the selective dimerisation of ethylene utilising methylaluminoxane (MAO) as a cocatalyst. Furthermore, when **1.a** was supported and methylated *in situ* on solid polymethylaluminoxane^{10,11} (sMAO) the resulting solid catalyst was ~7 times more active in the slurry phase than its homogeneous analogue (Chart 1, sMAO-1.a).¹²

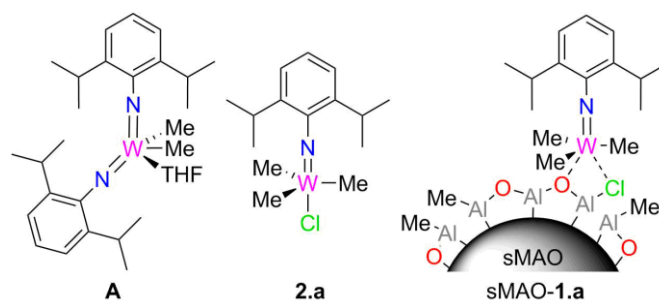


Chart 1. Previously reported well-defined homogeneous and heterogeneous tungsten diisopropylphenylimido oligomerisation catalysts.^{8,12}

Chemistry Research Laboratory, Department of Chemistry, University of Oxford, 12 Mansfield Road, Oxford, OX1 3TA U.K.

* Email: dermot.ohare@chem.ox.ac.uk

Electronic Supplementary Information (ESI) available: [Crystallographic data tables for **1.1-1.7**, **2.1-2.3**, **2.5** and **2.6**. Solid Angle calculations and spacefilled models, solution NMR and FTIR spectroscopy of the homogeneous complexes (**1.1-1.7**, **2.1-2.7**), solid state NMR and FTIR spectroscopy and ICP-MS analysis of the supported complexes (sMAO-**1.1-1.7**, sMAO-**2.6***, structure activity correlations, 1-hexene/1-octene oligomerisation data, complex loading study and solvent polarity/donor properties table (PDF). Crystallographic information files for **1.1-1.7** and **2.1**, **2.2**, **2.3**, **2.5** and **2.6** (cif).]

See DOI: 10.1039/x0xx00000x

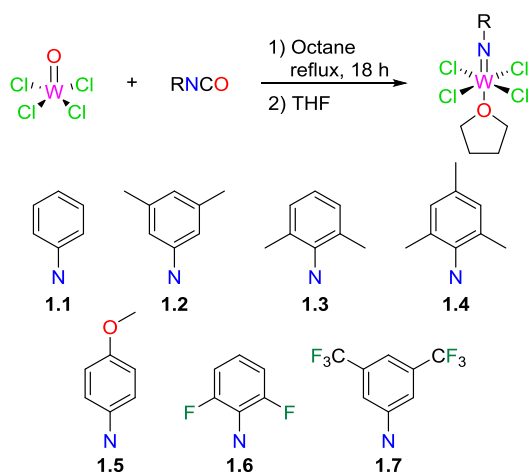
Selective ethylene oligomerisation is an important reaction especially in the area of hydrocarbon upgrading.¹³ Products of dimer-, trimer- and tetramerisation find significant use as co-monomers in polyethylene production.¹⁴ Work on ethylene oligomerisation catalysts utilising PCP pincer chromium complexes has shown that variation of the PCP ligand backbone can switch catalyst selectivity from trimerisation to tetramerisation.¹⁵ Work by Copéret and co-workers on silica-supported tungsten imido complexes of the type $W(NAr)(CHCMe_2R)(X)$ ($Ar = 2,6\text{-}^i\text{Pr-C}_6\text{H}_3$, $2,6\text{-Cl-C}_6\text{H}_3$, $2\text{-CF}_3\text{-C}_6\text{H}_4$, and C_6F_5 ; $X = OC(CF_3)_3$, $OCMe(CF_3)_2$, $O^t\text{Bu}$, $OSi(O^t\text{Bu})_3$, 2,5-dimethylpyrrolyl and $R = \text{Me}$ or Ph), allowed prediction of the activity for the self-metathesis of *cis*-4-nonene based on the steric and electronic properties of the imido and X ligands. High activity was associated with complexes containing X and imido ligands of opposite electronic character.¹⁶

Herein, we report the synthesis and characterisation of a variety of substituted tungsten mono-arylimido complexes of general formula $W(NR)Cl_4(THF)$ and $W(NR)Me_3Cl$. The $W(NR)Cl_4(THF)$ complexes have been immobilised on sMAO to yield solid catalysts for ethylene oligomerisation. The effect of variation of the stereoelectronic properties of the imido ligand in the supported catalysts has on the selectivity and activity towards ethylene oligomerisation has been probed, utilising the $W(NR)Me_3Cl$ complexes as homogeneous analogues.

Results and discussion

Synthesis and characterisation of $W(NR)Cl_4(THF)$ ($R = C_6H_5$ (1.1**),¹⁷ 2,6-Me- C_6H_3 (**1.2**),¹⁸ 3,5-Me- C_6H_3 (**1.3**), 2,4,6-Me- C_6H_2 (**1.4**), 4-OMe- C_6H_4 (**1.5**),¹⁹ 2,6-F- C_6H_3 (**1.6**) and 3,5- CF_3 - C_6H_3 (**1.7**)).**

Using a previously reported procedure,^{12,20} reaction of $W(O)Cl_4$ with aryl isocyanates in refluxing octane affords the corresponding arylimido complexes **1.1–1.7** (Scheme 1).



Scheme 1. Synthesis of $W(NR)Cl_4(THF)$ complexes.

These can be easily recrystallised, as single crystals suitable for an X-ray diffraction study, from coordinating solvents as the

solvent adduct which has an octahedral geometry about tungsten (Figure 1). Comparisons of the key structural and spectroscopic features of the molecular structures of **1.1–1.7** with literature examples, **1.a**, $W\{N(4\text{-Me-C}_6\text{H}_4)\}Cl_4(THF)^{21}$ (**B**), $W\{N(4\text{-I-C}_6\text{H}_4)\}Cl_4(NCMe)^{22}$ (**C**) and $Mo\{N(3,5\text{-CF}_3\text{-C}_6\text{H}_3)\}Cl_4(THF)^{23}$ (**D**) are shown in Tables 1 and S2. It can be seen from the $^{13}C\{^1H\}$ NMR spectroscopic resonances for the *ipso* carbon of the imido fragment and the pK_a values for the parent anilines^{24,25} that there is a large variation in the electronic properties as expected changing from electron donating to electron withdrawing substituents; pK_a values lying in the order 4-OMe > 3,5-Me > 4-Me > 2,4,6-Me > C_6H_5 > 2,6-Me > 2,6- ^iPr > 4- ^iPr > 3,5- CF_3 > 2,6-F closely mirroring the C_{ipso} resonances for the complexes: 4-OMe < 2,4,6-Me < 2,6-Me < C_6H_5 ≈ 3,5-Me < 3,5- CF_3 < 2,6- ^iPr < 2,6-F. From the calculated steric parameters it is clear that the diisopropylphenyl group is by far the most sterically demanding (Figure S1) with substitution at the 2,6-position leading to the largest percentage coverage of the metal center, measured at 2.28 Å from the tungsten center ($G_{2.28}(\text{imido})$).²⁶ Despite these factors, there is very little difference observed in the W-N bond lengths (1.711(3)–1.733(3) Å) between all the imido complexes. A noticeable change is observed in the W-N-C angle which moves away from linearity, especially for the 4-OMe (171.9(3)°) and the 3,5- CF_3 (172.9(3)°) substituted complexes; however, again this does not follow either the trends in steric parameters or electronics for the imido moieties. Comparison of **1.7** with its molybdenum analogue (**D**) shows the similarity between the two metals, due to their comparable atomic radii, owing to the lanthanide contraction.²⁷

A clearer trend can be observed by focusing on the unsubstituted phenyl and alkyl-substituted *aryl* imido groups. Increasing the number of substituents around the ring leads to a general increase in the W-N bond length **1.4** > **1.2** ≈ **1.3** > **B** ≈ **1.1** with all the W-N-C angles closer to linearity (176.0(3)–179.5(5)°) than the more electron withdrawing (**C** (174.4(9)°) or **1.7** (172.9(3)°)) or donating (**1.5** (171.9(3)°)) imido fragments. The sterically demanding 2,6- ^iPr group of **1.a** is the most electron deficient alkyl substituted *aryl* imido reflected in both its pK_a and δC_{ipso} making it more withdrawing than the unsubstituted **1.1** (4.00 and 156.1 ppm vs 4.64 and 149.6 ppm respectively).

NMR (1H , $^{13}C\{^1H\}$ and where applicable $^{19}F\{^1H\}$) spectra exhibit resonances corresponding to the aromatic imido protons, along with one equivalent of bound THF (Figures S16–31). FTIR spectra (Figures S47–53) for the complexes all display peaks around 3,000 cm^{-1} corresponding to aromatic C-H stretches, 1,500–1,400 cm^{-1} for aromatic C-C stretches, 1,335–1,250 cm^{-1} for the aromatic C-N stretch and 900–675 cm^{-1} for the C-H out of plane mode. W-N imido stretches are known to be weak in nature and overlapped by stretches from other ligands, making their assignment very difficult.²⁸

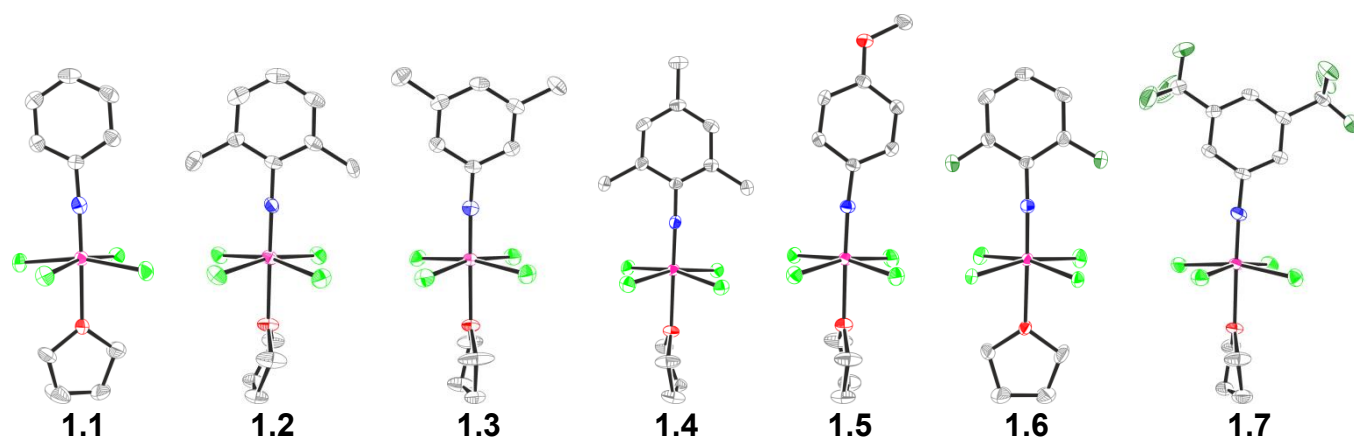


Figure 1. Molecular structures of the $W(NR)Cl_4(THF)$ complexes. Hydrogen atoms omitted for clarity, ellipsoids shown at 50% probability. $W\{N(C_6H_5)\}Cl_4(THF)$ (**1.1**), $W\{N(2,6-Me-C_6H_3)\}Cl_4(THF)$ (**1.2**), $W\{N(3,5-Me-C_6H_3)\}Cl_4(THF)$ (**1.3**), $W\{N(2,4,6-Me-C_6H_2)\}Cl_4(THF)$ (**1.4**), $W\{N(4-OMe-C_6H_4)\}Cl_4(THF)$ (**1.5**), $W\{N(2,6-F-C_6H_3)\}Cl_4(THF)$ (**1.6**) and $W\{N(3,5-CF_3-C_6H_3)\}Cl_4(THF)$ (**1.7**).

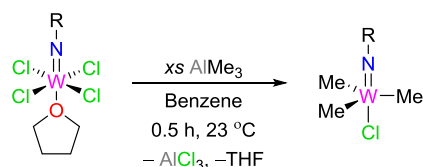
Table 1. Comparison of selected bond lengths (Å), angles (°), $^{13}C\{^1H\}$ C_{ipso} and where applicable $^{19}F\{^1H\}$ NMR spectroscopic chemical shifts (ppm), $G_{2,28}(imido)$ (%)²⁶ and pK_a values for the parent anilines²⁹ for $W(NR)Cl_4(THF)$ unless specified otherwise. Estimated standard deviations (ESDs) are given in parentheses.

Complex	R	W-N	W-N-C	δC_{ipso}^b	$^{19}F\{^1H\}$	$G_{2,28}(imido)^{26}$	$pK_a^{15}(RNH_3^+)^{29}$
B ²¹	4-Me-C ₆ H ₄	1.711(7)	178.38(1)	-	-	12.82	4.99
C ^{22, a}	4-I-C ₆ H ₄	1.723(9)	174.4(9)	-	-	12.74	3.86
D ²³	$Mo\{N(3,5-CF_3-C_6H_3)\}Cl_4(THF)$	1.711(3)	171.4(3)	152.8	-62.66	12.88	2.35
1.a ¹²	2,6- ⁱ Pr-C ₆ H ₃	1.723(3)	178.4(3)	156.1	-	18.62	4.00
1.1	C ₆ H ₅	1.717(4)	177.1(3)	149.6	-	12.76	4.64
1.2	2,6-Me-C ₆ H ₃	1.722(5)	179.5(5)	148.1	-	15.98	4.31
1.3	3,5-Me-C ₆ H ₃	1.722(3)	176.0(3)	149.6	-	12.77	5.07
1.4	2,4,6-Me-C ₆ H ₂	1.732(3)	177.4(3)	146.4	-	16.05	4.65
1.5	4-OMe-C ₆ H ₄	1.733(3)	171.9(3)	144.0	-	12.83	5.11
1.6	2,6-F-C ₆ H ₃	1.722(2)	176.22(18)	164.5	-111.04	13.99	0.69
1.7	3,5-CF ₃ -C ₆ H ₃	1.727(3)	172.9(3)	150.0	-63.08	12.88	2.35

^a Coordinating solvent NCMc. ^b $^{13}C\{^1H\}$ NMR in *d*₆-benzene.

Synthesis and characterisation of $W(NR)Me_3Cl$ complexes (R = C₆H₅ (**2.1**), 2,6-Me-C₆H₃ (**2.2**), 3,5-Me-C₆H₃ (**2.3**), 2,4,6-Me-C₆H₂ (**2.4**), 4-OMe-C₆H₄ (**2.5**), 2,6-F-C₆H₃ (**2.6**) and 3,5-CF₃-C₆H₃ (**2.7**)).

All $W(NR)Cl_4(THF)$ (**1.1-1.7**) complexes detailed previously were reacted with trimethyl aluminium (TMA) to yield the trigonal bipyramidal $W(NR)Me_3Cl$ complexes in the same manner as previously reported (Scheme 2).¹²



Scheme 2. Synthesis of $W(NR)Me_3Cl$ complexes.

Recrystallisation from hexane at -33 °C allowed for elucidation of the solid-state molecular structures of five of these complexes (**2.1-2.3**, **2.5** and **2.6**) (Figure 2). The key structural and spectroscopic details for the isolated complexes are given in Table 2. For this set of complexes the change in the W-N bond length reflects the change in the electronics of the imido group, following the order of the pK_a values for the parent

anilines with the most electron deficient moieties exhibiting the longest bonds. An increase in the W-N-C angle is noted as the size of the substituents in the 2,6- positions are increased and is attributed to the steric clash between these and one of the methyl groups. Elongation of the W-Cl bond *trans* to the imido group compared to that seen for the W-Cl bonds in the corresponding $W(NR)Cl_4(THF)$ complexes indicates increased lability of this bond. From the SolidAngle calculations,²⁶ it is clear that the methyl groups provide little steric protection towards the axial chloride ligand, making activation of this bond more facile (Figure S2).

1H and ^{19}F (where applicable) NMR spectra (Figures S32-46) show a shift to lower frequency in the imido resonances compared to the $W(NR)Cl_4(THF)$ complexes and a new singlet resonance in the 1H NMR spectrum accompanied by tungsten satellites between 1.24-1.41 ppm corresponding to the formation of three W-Me bonds and hence a more electron rich complex. The W-Me groups in **2.7** are far more shielded than expected for a withdrawing imido group, the 1H NMR spectroscopic resonance for the methyl groups appears at 1.24 ppm, the lowest value for the range of complexes.

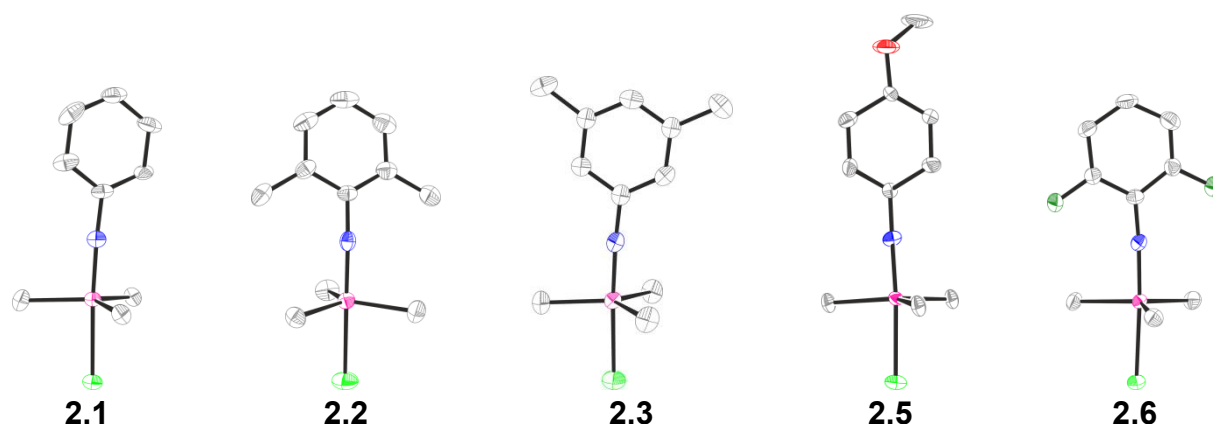


Figure 2. Molecular structures of the W(NR)Me₃Cl complexes. Hydrogen atoms omitted for clarity, ellipsoids shown at 50% probability. W{N(C₆H₅)}Me₃Cl (**2.1**), W{N(2,6-Me-C₆H₃)}Me₃Cl (**2.2**), W{N(3,5-Me-C₆H₃)}Me₃Cl (**2.3**), W{N(4-OMe-C₆H₄)}Me₃Cl (**2.5**) and W{N(2,6-F-C₆H₃)}Me₃Cl (**2.6**).

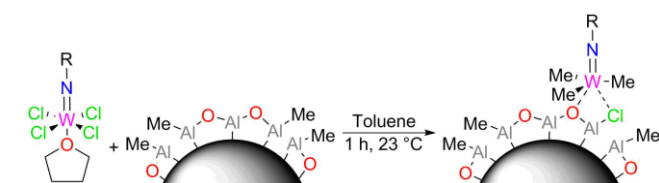
Table 2. Comparison of selected bond lengths (Å), angles (°), ¹³C{¹H} C_{ipso}, ¹H W-Me and where applicable ¹⁹F{¹H} NMR spectroscopic chemical shifts (ppm) and G_{2.28}(imido) (%)²⁶ for the synthesised W(NR)Me₃Cl complexes and relevant literature compounds. Estimated standard deviations (ESDs) are given in parentheses.

Complex	R	W-N	W-Cl	W-C _α (av.)	W-N-C	δ C _{ipso} ^a	δ W-Me	¹⁹ F{ ¹ H}	G _{2.28} (imido) ²⁶
A ⁸	W{N[2,6- ⁱ Pr-C ₆ H ₃]} ₂ Me ₂ (THF)	1.764(4) ^b	-	2.158(5)	176.9(4) ^b	152.8	1.25	-	-
E ³⁰	Mo{N[2,6- ⁱ Pr-C ₆ H ₃]} ₂ Me ₂	1.749(4) ^b	-	2.109(5)	159.6(3) ^b	153.09	1.39	-	-
F ²³	Mo{N(3,5-CF ₃ -C ₆ H ₃)}Np ₃ Cl	1.7471(17)	2.3944(5)	2.142(16)	174.94(15)	-	-	-62.49	-
2.a ¹²	2,6- ⁱ Pr-C ₆ H ₃	1.743(9) ^c	2.414(3) ^c	2.108(12) ^c	172.0(6) ^c	150.4	1.41	-	18.47
2.1	C ₆ H ₅	1.740(8)	2.415(2)	2.109(9)	174.9(6)	152.1	1.29	-	12.79
2.2	2,6-Me-C ₆ H ₃	1.746(4)	2.4324(14)	2.098(5)	171.7(3)	150.4	1.34	-	15.99
2.3	3,5-Me-C ₆ H ₃	1.731(8)	2.404(3)	2.100(8)	176.3(7)	152.3	1.34	-	12.77
2.4	2,4,6-Me-C ₆ H ₂	-	-	-	-	149.0	1.41	-	-
2.5	4-OMe-C ₆ H ₄	1.737(10)	2.416(2)	2.106(8)	178.0(3)	159.7	1.30	-	12.76
2.6	2,6-F-C ₆ H ₃	1.753(4)	2.4239(13)	2.103(5)	174.8(4)	163.9	1.45	-117.56	13.96
2.7	3,5-CF ₃ -C ₆ H ₃	-	-	-	-	153.2	1.24	-62.88	-

^a ¹³C{¹H} NMR in *d*₆-benzene. ^b Calculated for the linear imido fragment. ^c Average of the two molecules in the asymmetric unit cell. Np = neopentyl.

Immobilisation and characterisation of W(NR)Cl₄(THF) on solid polymethylaluminoxane^{10,11} (sMAO).

Supporting W{N[2,6-ⁱPr-C₆H₃]}Cl₄(THF) (**1.a**) on solid polymethylaluminoxane (sMAO),^{10,11} has been shown to yield an active catalyst for the selective dimerisation of ethylene (sMAO-**1.a**), with results indicating that methylation of the chloride groups occurred *in situ* during grafting.¹² The sMAO support, formed from the reaction of TMA with benzoic acid followed by heat treatment to yield an insoluble MAO, has also shown great success in supporting and activating metallocene type ethylene polymerisation catalysts.^{11,31,32} The synthesised W(NR)Cl₄(THF) were supported as described previously (W:Al = 1:150) utilising the concept of surface organometallic chemistry (SOMC) (Scheme 3).³³



Scheme 3. SOMC³³ grafting procedure for arylimido complexes on sMAO.

An immediate colour change was observed in all cases upon mixing of W(NR)Cl₄(THF) and sMAO in toluene, with formation of a coloured solid and a clear solution after one hour of swirling. The suspensions were filtered and dried to yield pale coloured powders in quantitative yield in all cases. Immobilisation of **1.3** on sMAO was also conducted on an NMR spectroscopic scale in *d*₆-benzene (Al/W = 150). Total disappearance of the resonances corresponding to the molecular complex was observed, indicative of complete grafting of the complex onto the solid surface, with a small quantity of methane evolution observed.

Solid-state NMR and FTIR spectroscopy have been used to identify the surface species (Figures S58-74). The solid-state ¹⁹F{¹H} MAS NMR spectrum (Figure 3) of sMAO-**1.6** indicates homogeneity in the surface supported species with only one resonance observed (-122.52 ppm). This is shifted to lower frequency with respect to both W{N(2,6-F-C₆H₃)}Cl₄(THF) (**1.6**) and W{N(2,6-F-C₆H₃)}Me₃Cl (**2.6**) (-111.04 and -117.56 ppm respectively) but lies in the region of the methylated complex resonance, further supporting that methylation of the compound has occurred on the surface.¹²

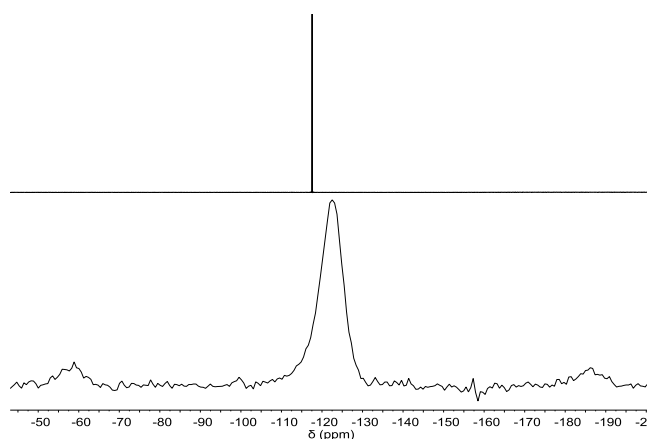


Figure 3. Solution and solid-state $^{19}\text{F}\{^1\text{H}\}$ NMR spectra of **2.6** (top) and sMAO-1.6 (bottom).

A broad resonance at 67 ppm is observed in the $^{13}\text{C}\{^1\text{H}\}$ CPMAS solid-state NMR spectrum which we attribute to a combination of THF and W-Me resonances of the supported species compared to **2.6** where the W-Me resonances are observed at 54.44 ppm in solution (Figures S60 and S43). Ghiotto *et al.* have previously reported that addition of THF to MAO solutions leads to dissociation of $[\text{AlMe}_2(\text{THF})_2]^+$ cations, observed by ^1H NMR spectroscopy.³⁴ The resonance for such species is seen to shift from -0.3 ppm towards -0.7 ppm dependent on the concentration of THF. We have previously shown analysis of sMAO-1.a by ^1H NMR spectroscopy in d_8 -THF led to observed leaching of **2.a** with an observable shift in the resonance at -0.60 ppm for the 'bound' TMA in the initial sMAO structure to -0.76 ppm, proposed to result from similar aluminium cation formation.^{11,12}

The $^{19}\text{F}\{^1\text{H}\}$ MAS NMR spectrum of sMAO-1.7, (Figure 4) shows the presence of two fluorine environments at -69 and -141 ppm, the former is assigned to the surface-supported complex. The large shift to lower frequency of the latter resonance infers that C-F activation may have also occurred, with transfer of the fluoride onto the surface aluminium species (Scheme 4). Work by Grey and co-workers involving the surface fluorination of alumina has demonstrated that the surface Al-F species display ^{19}F MAS NMR resonances between -110 and -165 ppm.³⁵ Terao *et al.* have described how the C-F bonds of various benzotrifluorides could be converted to C-Me bonds using excess AlMe_3 .³⁶ Despite the large excess of sMAO, the fact that the complex is immobilised may be why complete defluorination of the complex is not observed.

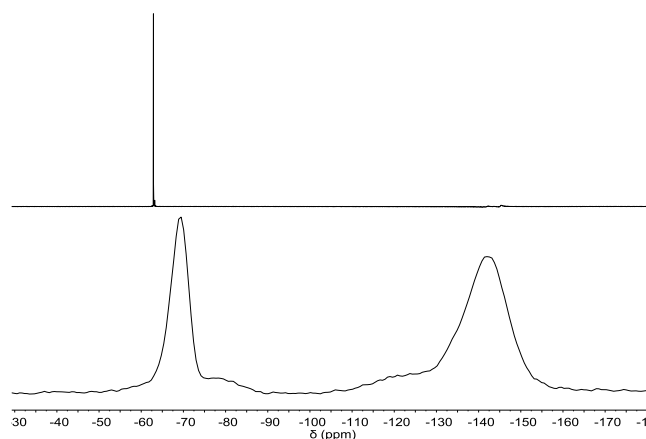
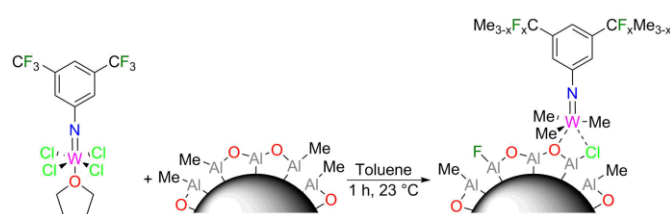


Figure 4. Solution and solid-state $^{19}\text{F}\{^1\text{H}\}$ NMR spectra of **1.7** (top) and sMAO-1.7 (bottom).



Scheme 4. Proposed species formed from the reaction of **1.7** and sMAO, with exchange of fluorine atoms from the CF_3 groups with surface methyl groups bound to aluminium.

To try and further understand the nature of the supported species, $\text{W}\{\text{N}(2,6\text{-F-C}_6\text{H}_3)\}(\text{C}(\text{CH}_3)_3)_3\text{Cl}$ (**2.6***) was synthesised utilising ^{13}C -enriched TMA as the methylating reagent. The complex was then reacted with sMAO and the resulting pale yellow solid studied by solid-state NMR spectroscopy. The $^{13}\text{C}\{^1\text{H}\}$ CPMAS NMR spectrum displays two discernable resonances, a weaker resonance at 45 ppm and a stronger resonance at 56 ppm (Figure S62), the latter matching almost exactly with **2.6***. Neither of these is as strong as may have been anticipated for a labelled complex which may be due to methyl exchange with the surface and hence loss of intensity. The two resonances are proposed to arise due to the asymmetry of the methyl environments of the immobilised complex. Such a splitting of the methyl resonances is observed in the $^{13}\text{C}\{^1\text{H}\}$ CPMAS $\{^{19}\text{F}\}$ decoupled solid-state NMR spectrum of **2.6** (Figure S64). The difference observed between the W-Me resonances for sMAO-**2.6*** and that of sMAO-**1.6** (67 ppm) may be due to the fact that the chlorides deposited in close proximity to the complex on the surface have an interaction with the metal centre rendering it electron deficient and hence deshielding the methyl groups; we have previously attributed the W-Al-Cl interaction to the increased stability of the complexes on the surface.¹² The $^{19}\text{F}\{^1\text{H}\}$ MAS solid-state NMR spectrum of sMAO-**2.6*** (Figure 5) displays a single fluorine environment centered at -123.36 ppm which is similar to that observed for sMAO-**1.6**.

In all of the above cases, the ^{27}Al Hahn echo spectra (ESI) displayed a broad set of resonances between 500 and -500 ppm characteristic of the sMAO support.¹¹

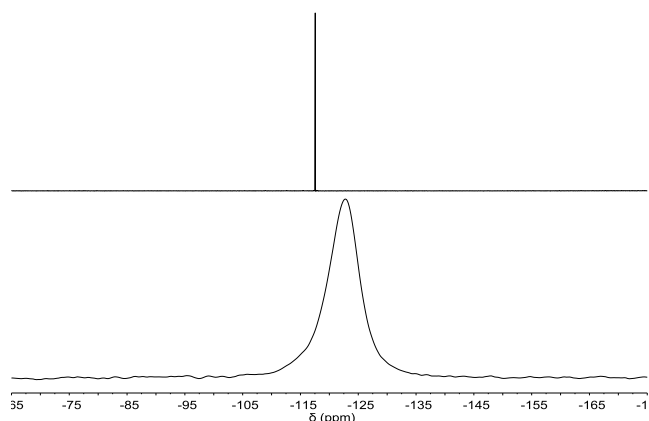


Figure 5. Solution and solid-state $^{19}\text{F}\{^1\text{H}\}$ NMR spectra of **2.6*** (top) and **sMAO-2.6*** (bottom).

FTIR spectroscopy of the supported catalysts was compared with the homogeneous complexes (ESI). Due to the low loading and generally weak absorptions of the complexes, the spectra for the supported species are dominated by absorptions from the sMAO support. An increase in intensity for the broad band between 500 and 900 cm^{-1} was observed in all cases.

Catalytic Testing

To test the capability of the supported catalysts towards ethylene oligomerisation, the solid catalysts (W:Al = 1:150) were reacted at 100 °C in d_6 -benzene with 1 bar ethylene (Figure 6). The results indicate that electron deficient imido groups yield the most active catalysts with **sMAO-1.7** displaying the highest turnover numbers (63 $\text{mol}_{\text{C}_2\text{H}_4}\text{mol}^{-1}\text{W}$ after 12 hours). This has previously been seen in homogeneous propene oligomerisation reactions using $\text{W}(\text{NR})\text{Cl}_4(\text{THF})$ complexes and diethylaluminium chloride as a cocatalyst where activity fell in the order $\text{R} = 4\text{-F-C}_6\text{H}_4 > \text{C}_6\text{H}_5 > 2,6\text{-Me-C}_6\text{H}_3 > 2,6\text{-}^i\text{Pr-C}_6\text{H}_3$.⁹

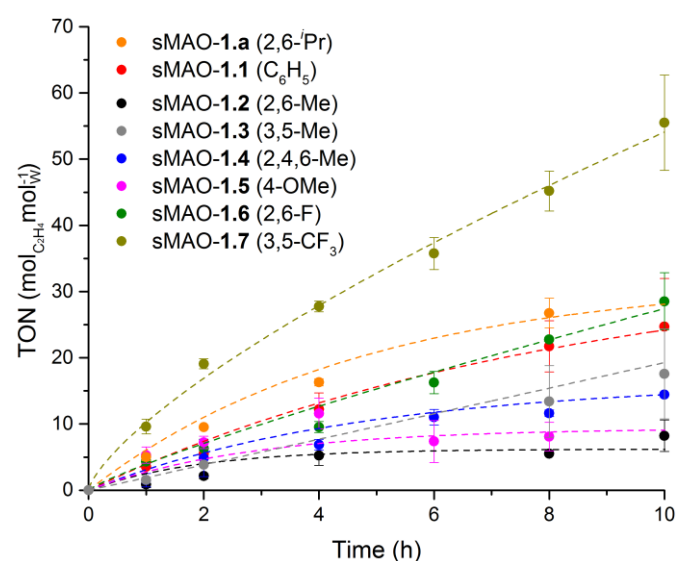


Figure 6. Turnover numbers (TONs) of ethylene for the various sMAO-supported tungsten arylimido complexes at 100 °C, 1 bar ethylene, d_6 -benzene and W:Al = 1:150.

Table 3. Turnover frequencies (TOFs) and selectivities towards 1-butene for the various sMAO-supported catalysts.

Complex	R	TOF ^a ($\text{mol}_{\text{C}_2\text{H}_4}\text{mol}^{-1}\text{W h}^{-1}$)	Selectivity towards 1-butene ^a (%)
sMAO-1.a	2,6- ⁱ Pr-C ₆ H ₃	3.34	79
sMAO-1.1	C ₆ H ₅	2.72	87
sMAO-1.2	2,6-Me-C ₆ H ₃	0.69	69
sMAO-1.3	3,5-Me-C ₆ H ₃	1.68	68
sMAO-1.4	2,4,6-Me-C ₆ H ₂	1.45	81
sMAO-1.5	4-OMe-C ₆ H ₄	1.01	77
sMAO-1.6	2,6-F-C ₆ H ₃	2.86	71
sMAO-1.7	3,5-CF ₃ -C ₆ H ₃	5.65	91

^a Calculated after 8 hours.

It should be noted that the activity of the system presented here is significantly lower than the homogeneous system ($\text{TON} = 22,300 \text{ mol}_{\text{C}_2\text{H}_4}\text{mol}^{-1}\text{W}$ for the $\text{W}\{\text{N}(2,6\text{-Me-C}_6\text{H}_3)\}\text{Cl}_4$ and AlEt_2Cl system, $\text{Al}/\text{W} = 40$). However, much milder conditions have been employed in this study (1 vs 60 bar ethylene). Kermagoret *et al.* have described a supported nickel catalyst for selective ethylene dimerisation by contacting $\text{NiCl}_2(\text{PBU}_3)_2$ with silica-supported dimethylaluminium chloride (DEAC). Turnover frequencies as high as $498,000 \text{ mol}_{\text{C}_2\text{H}_4}\text{mol}^{-1}\text{Ni h}^{-1}$ with 95% selectivity for 1-butenes have been reported utilising MCM-41 silica (5 bar ethylene, 30 °C, $\text{Al}/\text{Ni} = 10$).³⁷ Interestingly, the trialkylaluminium-supported species show no activity for this reaction.³⁸ DEAC may lead to higher activities for this reaction but we have previously observed that reaction of **1.a** with ethylaluminium compounds resulted in formation of ill-defined species, with ethane evolution observed.¹²

Whilst a more electron withdrawing group may destabilise the proposed cationic transition state formed from halide or methyl abstraction, it will increase its affinity to bind ethylene and stabilise a propagating chain. The observed C-F activation of **sMAO-1.7** could also contribute to its enhanced reactivity. Kaminsky and co-workers have reported that fluorinated half-sandwich titanium complexes show an increase in activity for styrene polymerisation of up to 50 times with MAO as a co-catalyst compared to the chlorinated analogues.³⁹ Marks and co-workers have also demonstrated that a bulky (perfluoroaryl)fluoroaluminate counterion can stabilise metallocene cations *via* an Al-F-M interaction.^{40,41} Interestingly, the bulky $\text{W}\{\text{N}(2,6\text{-}^i\text{Pr-C}_6\text{H}_3)\}\text{Cl}_4(\text{THF})$ supported complex (**sMAO-1.a**) also displays relatively high turnover numbers of ethylene similar to that of the supported 2,6-fluorophenyl and phenyl imido complexes (**sMAO-1.6** and **sMAO-1.1** respectively). We attribute this to the increased steric bulk and a more electron deficient imido fragment, which may enhance the rate of β -hydride elimination of 1-butene, inhibiting further chain propagation. A statistical correlation ranking of steric and electronic factors vs the turnover frequency (TOF) calculated after 8 hours for **sMAO-1.a** and **sMAO-1.1-1.7** (Table 3 and S4), showed the strongest correlation between pKa values for the parent

anilines (Pearson's $r = -0.58$), but essentially no correlation between the steric factors indicating that it is the electronics of the imido substituent that is the dominating factor. Comparison of the sterics and electronics of the phenyl and four alkyl-substituted *ary*l imido groups (sMAO-(**1.1-1.4**) and sMAO-**1.a**) with the TOF shows an even stronger correlation (Pearson's $r = 0.81$) between the C_{ipso} resonance of the $W(NR)Cl_4(THF)$ complexes and the TOF for the supported catalysts (Table S5). The selectivity of all the catalysts towards 1-butene compared to isomerisation and metathesis to form propylene show no clear correlation with either the steric or electronic properties of the imido complexes. It should be noted that no higher oligomers were observed but in most cases a small amount of polyethylene formation was observed (1-2 mg). As no further reactivity with 1-butene was observed, reaction of sMAO-**1.6** (W:Al = 1:150) with the longer chain linear alpha olefins 1-hexene and 1-octene was attempted to ascertain whether the scope of the olefin monomer was limited to ethylene. Reactions were performed at 75 °C in d_6 -benzene and in both cases isomerisation reactions occurred yielding the internal olefins with near complete conversion (>91%) after heating for 4 hours (Figures S75 and S76). This suggests that olefin binding to the complex can occur. However, a second olefin is not able to insert to propagate the chain and hence isomerisation to the more stable internal isomers occurs.

Temperature study. Figure 7 depicts a temperature study utilising sMAO-supported $W\{N(4-OMe-C_6H_4)\}Cl_4(THF)$ (sMAO-**1.5**). The rate of butene formation is observed to increase with increasing temperature from 50 to 75 °C; with TONs after 24 h of 38 and 46 $mol_{C_2H_4}mol^{-1}_W$ respectively. At 100 °C the conversion of ethylene drops rapidly after 4 h. This is likely due to a change of reaction pathway from oligomerisation to polymerisation with polymer formed after 4 h. Additionally, colouring of the solution over time is characteristic of leaching of the complex from the sMAO support, something observed to a greater extent at higher temperatures. Selectivities towards 1-butene are considerably higher in the heterogeneous phase compared with the homogeneous phase. However, selectivity decreases as temperature increases; 72, 85 and 89% at 100, 75, and 50 °C respectively. The presence of butane, ethane, and methane indicated in the 1H NMR spectra suggests that there may be a tungsten hydride species being formed as part of the catalytic cycle which would imply a Cossee type mechanism.⁴² The lower selectivity for 1-butene due to isomerisation indicates that ethylene insertion into this hydride is relatively slow and thus competing 1-butene insertion and isomerisation can occur. Metallocycle formation for selective ethylene dimerisation has been demonstrated for tantalum systems; formation of the metallocycloheptane is disfavoured, hence sterically demanding β -hydride elimination from the tantalacyclopentane selectively yields 1-butene.⁴³⁻⁴⁵ Such a mechanism has previously been suggested for tungsten initiators displaying high selectivity in dimerisation,⁹ and a DFT study on mono-imido complexes activated by MAO concluded

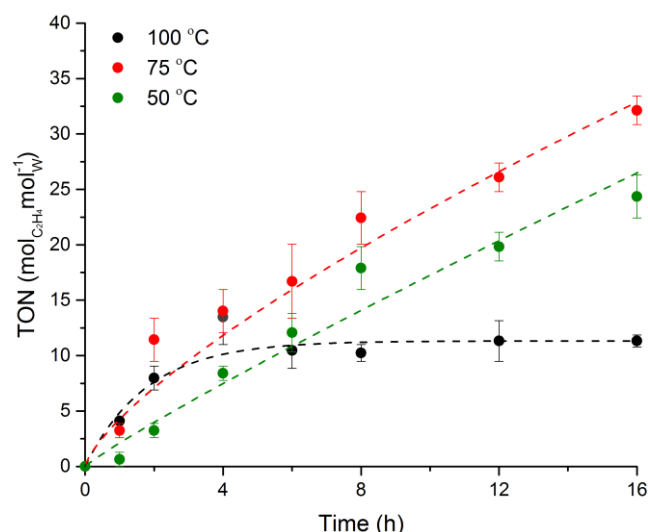


Figure 7. Temperature study using sMAO-**1.5** at 50, 75 and 100 °C with 1 bar ethylene, d_6 -benzene and W:Al = 1:150.

that such a route was feasible.⁴⁶ However, oligomerisation reactions with a mixture of C_2H_4/C_2D_4 (1:1) and either the $WCl_6/Et_3N/PhNH_2/AlEt_2Cl$ system or bis-imido system **A** have shown complete scrambling of the resulting oligomer, indicative of a Cossee mechanism.^{7,8}

Reaction of sMAO-**1.7** was also conducted at 75 °C (Figure S77) and showed a slight increase in activity compared to the reaction at 100 °C (TONs of 55 and 45 $mol_{C_2H_4}mol^{-1}_W$ after 8 h) indicative of higher thermal stability of this immobilised complex compared to sMAO-**1.5**. The complex is still active after longer reaction times (24 h) with the gradual decrease in activity attributed to near complete conversion of ethylene and hence a concentration effect.

Solvent Effects. Comparison of our previously reported results of sMAO-**1.a** utilising pyridine as an internal standard vs mesitylene highlights the effects that solvents have on the system (turnover numbers of 88 and 27 $mol_{C_2H_4}mol^{-1}_W$ after 16 and 14 hours respectively).¹² To further probe this effect a study was undertaken employing sMAO-**1.5** at 75 °C with variation of the deuterated NMR solvent: d_5 -chlorobenzene, d_5 -bromobenzene d_6 -benzene, d_8 -toluene, d_8 -THF, d_2 -DCM and d_{18} -octane (Figure 8 and Table 4).

The highest rates of oligomerisation are observed with polar aromatic solvents, with d_5 -chlorobenzene leading to the highest turnover numbers. This is likely to be due to two main factors. Firstly, in the catalytic cycle the postulated transition state after halide abstraction involves a positive charge on the metal centre. If the solvent can stabilise this positive charge through dipolar interactions, then it will result in a lower activation energy and so higher rates of oligomerisation. However, if the solvent coordinates to the metal, blocking a coordination site, it will prevent the metal species from being catalytically active and so reduce the rates of oligomerisation. A table of dielectric constants and donor numbers are shown in Table S7.^{47,48}

For non-coordinating solvents (those with a low donor number) the trend in the rates of oligomerisation increase

with the increase in polarity; d_{18} -octane > d_6 -benzene >

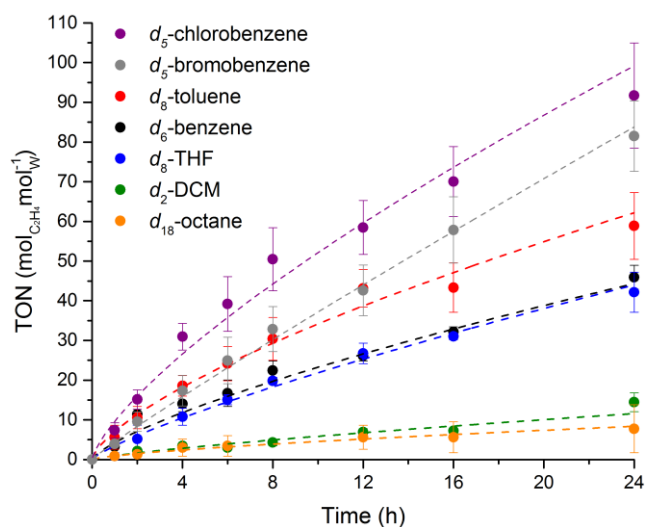


Figure 8. Effect of varying the solvent in the oligomerisation reaction using sMAO-1.5 at 75 °C, 1 bar ethylene and W:Al = 1:150.

Table 4. Turnover frequencies (TOFs) and selectivities towards 1-butene for sMAO-1.5 with variation of the solvent medium.

Solvent	TOF ^a (mol _{C₂H₄} mol ⁻¹ W ⁻¹ h ⁻¹)	Selectivity towards 1-butene ^a (%)
d_{18} -octane	0.57	>99
d_6 -benzene	2.8	84
d_8 -toluene	3.8	91
d_5 -chlorobenzene	6.31	90
d_5 -bromobenzene	4.11	85
d_8 -THF	2.48	>99
d_2 -DCM	0.54	>99

^a Calculated after 8 hours.

d_8 -toluene > d_5 -bromobenzene > d_5 -chlorobenzene (TOFs of 0.57, 2.8, 3.8, 4.11 and 6.31 mol_{C₂H₄}mol⁻¹W⁻¹h⁻¹ respectively after 8 h). In exception to this, attempted reaction in d_4 -1,2-dichlorobenzene resulted in deactivation of the catalyst yielding a bright red solid that displayed low activity for the oligomerisation reaction (TOF = 1.18 mol_{C₂H₄}mol⁻¹W⁻¹h⁻¹ after 8 h). However, d_8 -THF and d_2 -DCM can both coordinate to the metal center through interactions of lone pairs of electrons on the heteroatoms blocking olefin coordination. For d_8 -THF the balance between its higher polarity and donor ability results in a solvent medium similar to that of d_6 -benzene. For d_2 -DCM reaction with the support was observed, with a change in colour of the support and colouring of the solution indicating that decomposition had occurred. A high level of selectivity towards 1-butene is observed for all of the solvents employed in this study ($\geq 84\%$). Work by Bercaw and co-workers employing bis(diphenylphosphino)amine ligands in chromium catalysed ethylene oligomerisation, showed that variation of the solvent medium from toluene to the more polar chlorobenzene resulted in higher activity, stability and selectivity towards trimer- and tetramerisation, with reduced polymer formation.⁴⁹ Variation of the reaction solvent by

Hanton *et al.* on the ill-defined WCl₆, PhNH₂, Et₃N and EtAlCl₂ system yielded similar results, with chlorobenzene the most active medium for 1-hexene dimerisation and donor solvents (THF, MeCN) inhibiting the reactivity.⁷

Loading study. The loading of **1.5** on sMAO was varied (W:Al = 1:100, 1:150 and 1:200) with the resulting oligomerisation reactions showing that a W:Al of 1:150 has the highest activity followed by 1:200 with 1:100 3 times less active (TONs of 22.4, 15.5 and 6.5 mol_{C₂H₄}mol⁻¹W⁻¹ respectively after 8 hours) (Figure S78). Selectivities towards 1-butene over the loading range remain constant ($\sim 85\%$). At high loadings of tungsten (1:100), blocking of the active sites and bimetallic decomposition pathways may be facilitated due to the close proximity of the immobilised complexes.

Conclusions

A series of tungsten mono-arylimido complexes of the type W(NR)Cl₄(THF) (R = C₆H₅ (**1.1**), 2,6-Me-C₆H₃ (**1.2**), 3,5-Me-C₆H₃ (**1.3**), 2,4,6-Me-C₆H₂ (**1.4**), 4-OMe-C₆H₄ (**1.5**), 2,6-F-C₆H₃ (**1.6**) and 3,5-CF₃-C₆H₃ (**1.7**)) bearing different substituents on the phenyl ring have been synthesised and fully characterised. Subtle changes in the molecular structures are observed based on the electronic properties and steric effects which are most notable in the 2,6-position. Reaction of these complexes with TMA led to methylation of three of the chloride positions and a structural change from octahedral to trigonal bipyramidal geometry to yield the corresponding W(NR)Me₃Cl complexes **2.1-2.7**. Changes in the W-N bond length match the electronic properties of the imido fragments determined indirectly from the pK_as of their parent anilines.

W(NR)Cl₄(THF) complexes have been supported on solid polymethylaluminoxane (sMAO-**1.1-1.7**) with solid-state ¹³C-{¹H} CPMAS NMR spectroscopy indicating that methylation of the complex occurs *in situ* during grafting. This was further validated by comparison of the ¹³C-{¹H} and ¹⁹F-{¹H} NMR spectra of **2.6** and sMAO-**2.6** with the ¹³C-{¹H} CPMAS and ¹⁹F-{¹H} MAS SSNMR spectra of W{N(2,6-F-C₆H₃)}(¹³CH₃)₃Cl (**2.6***) immobilised on sMAO (sMAO-**2.6***).

In all cases the sMAO-supported complexes are active for the selective dimerisation of ethylene to yield predominantly 1-butene. It was observed that electron withdrawing imido groups displayed the highest turnover numbers with sMAO-W{N(3,5-CF₃-C₆H₃)}Cl₄(THF) (sMAO-**1.7**) the most active and selective (TOF of 5.65 mol_{C₂H₄}mol⁻¹W⁻¹h⁻¹ after 8 hours and 91% selectivity towards 1-butene). Markedly, of all the alkyl substituted aryl imido catalysts, the diisopropylphenylimido moiety yielded the highest activity which is attributed to the steric demand and more electron deficient nature of this group (seen in both the pK_as of the parent anilines and C_{ipso} resonances for the complexes) and potentially increasing rates of β -hydride elimination. Utilising sMAO-**1.5**, solvent, temperature and loading studies led to optimisation of the reaction conditions (d_5 -chlorobenzene, 75 °C and W:Al = 1:150). For non-coordinating solvents activity was seen to increase with polarity, and high temperatures and loadings

seen to shut down reactivity which may be indicative of decomposition.

Experimental section

All reactions were performed under an inert N₂ atmosphere using standard Schlenk line techniques and, where required, an MBraun UNILab glovebox. Pentane, hexane, benzene, DCM and toluene were dried and degassed using an MBraun SPS-800 solvent purification system. Octane was dried over 4 Å molecular sieves for a minimum of 24 hours. Mesitylene was dried by refluxing under reduced pressure over sodium. THF was distilled from Na/benzophenone and diethylether was distilled from Na/K. All solvents were stored in Rotaflo ampoules either over a potassium mirror (pentane, hexane, octane, toluene and diethyl ether) or 4 Å molecular sieves (benzene, DCM, THF and mesitylene) and degassed under partial vacuum before use. *d*₆-Benzene (Sigma Aldrich), *d*₈-toluene, *d*₂-DCM and *d*₁₈-octane (Goss Scientific) and *d*₈-THF (Fluorochem) were dried at reflux under partial vacuum either over K (*d*₆-benzene, *d*₈-toluene and *d*₁₈-octane) or CaH₂ (*d*₂-DCM and *d*₈-THF). They were freeze-pump-thaw degassed three times and stored under N₂. Solution samples for NMR spectroscopy were made up in the glovebox, using 5 mm Young's tap NMR tubes. Spectra were recorded either on a Bruker Avance III HD Nanobay 400 MHz NMR spectrometer at 298 K and were referenced to the residual protio-solvent peak. ¹³C{¹H} NMR assignments were confirmed by 2D correlation experiments (HSQC and HMBC). Solid-state NMR spectra were recorded on a Bruker Avance III HD Nanobay 400 MHz NMR spectrometer in 4 mm OD rotors using contact times for CPMAS spectra of 3000 μs. Samples were spun at the magic angle (54.71°) at spin rates of 10 kHz and referenced to adamantane (¹³C), teflon (¹⁹F) or Al(NO₃)₃ (²⁷Al).

Air-sensitive IR samples were prepared in the glove box as pressed KBr discs. Spectra were recorded on a Nicolet iS5 ThermoScientific spectrometer in transmission mode (range 4000-400 cm⁻¹, resolution 1 cm⁻¹).

Crystals were mounted on MiTeGen MicroMounts using perfluoropolyether oil and rapidly transferred to a goniometer head on a diffractometer fitted with an Oxford Cryosystems Cryostream open-flow nitrogen cooling device.⁵⁰ Data collections were carried out at 150 K either using an Oxford Diffraction Supernova diffractometer using mirror-monochromated Cu Kα radiation (λ = 1.54184 Å) with data processed using CrysAlisPro⁵¹ or using an Enraf-Nonius Kappa CCD diffractometer using graphite-monochromated Mo Kα radiation (λ = 0.71073 Å), where raw frame data were reduced using the DENZO-SMN package,⁵² and corrected for absorption using SORTAV.⁵³ The structures were solved using direct methods (SIR-92)⁵⁴ or a charge-flipping algorithm (SUPERFLIP)⁵⁵ and refined by full-matrix least-squares procedures using the Win-GX software suite.^{56,57}

Elemental analysis (CHN) was performed by Mr. Stephen Boyer at London Metropolitan University, North Campus, Holloway Road, London, N7 8DB.

Samples for ICP-MS were run in triplicate and were prepared by digestion in high purity HNO₃ solution (2 h reflux), and dilution with 18.2 Mohm DI water, calibrated using external calibration analysis (single element solutions of ²⁷Al and ¹⁸²W, ¹⁸⁴W and ¹⁸⁶W were obtained from Alfa Aesar and used to prepare a series of standards of known Al and ¹⁸²W, ¹⁸⁴W and ¹⁸⁶W concentrations which were measured externally to the samples to produce a linear calibration) and measured on an Agilent 7500 Series ICP-MS by Dr A. Abdul-Sada at the University of Sussex. An average of the results obtained for the three tungsten isotopes was taken and used to calculate individual Al/W ratios from which the percentage complex loading could be calculated.

WCl₆, TMA, ¹³CH₃I, phenyl isocyanate, 2,6-dimethylphenyl isocyanate, 4-methoxyphenyl isocyanate, 3,5-dimethylphenyl isocyanate were purchased from Sigma-Aldrich; 2,4,6-trimethylphenyl isocyanate, 2,6-difluorophenyl isocyanate and 3,5-bis(trifluoromethyl)phenyl isocyanate were purchased from Alfa Aesar. Isocyanates were freeze-pump-thaw degassed three times prior to use. The following compounds were synthesised according to literature procedures: solid polymethylaluminoxane,¹⁰ W(O)Cl₄,⁵⁸ W{N(2,6-*i*Pr-C₆H₃)}Cl₄(THF),²⁰ W{N(2,6-*i*Pr-C₆H₃)}Me₃Cl,¹² Al(¹³CH₃)₃.⁵⁹

General Procedure for the Synthesis of W(NR)Cl₄(THF) Complexes. The following syntheses were based on literature procedures.^{12,19,20} W(O)Cl₄ was added to a 500 mL all-in-one RBF condensor. Octane (250 mL) was added, followed by dropwise addition of 1.1 equivalents of the relevant phenylisocyanate reagent with stirring. The mixture was heated to reflux for 16 hours, after which it was allowed to cool to room temperature. The slurry was transferred to a Schlenk and the solvent removed by filtration. Drying of the resulting solid yielded powders in all cases. The solids were dissolved in THF resulting in a colour change and dried. Crystals suitable for single crystal X-ray diffraction studies were grown from hexane at -33 °C unless otherwise stated.

W{N(C₆H₅)}Cl₄(THF) (1.1). W(O)Cl₄ (5.0 g, 14.6 mmol) and phenyl isocyanate (1.9 g, 16.1 mmol) yielded W{N(C₆H₅)}Cl₄ (5.6 g) as a dark red solid in 92% yield. Dissolution in THF led to a dark green solution and a green solid after drying. Recrystallisation yielded green crystals of **1.1** in an isolated yield of 75%. Anal. Calcd (found) (%) C 24.57 (24.48), H 2.68 (2.61), N 2.87 (2.87). ¹H NMR (*d*₆-benzene) δ (ppm): 7.01 (d, 2H, ArH_{ortho}), 6.92 (t, 2H, ArH_{meta}), 6.17 (m, 1H, ArH_{para}), 4.47 (m, 4H, THF), 1.27 (m, 4H, THF). ¹³C{¹H} NMR (*d*₆-benzene) δ (ppm): 149.6 (Ar_{ipso}N), 133.9 (Ar_{para}H), 131.7 (Ar_{ortho}H), 127.2 (Ar_{meta}H), 73.9 (THF), 25.4 (THF).

W{N(2,6-Me-C₆H₃)}Cl₄(THF) (1.2). W(O)Cl₄ (5.0 g, 14.6 mmol) and 2,6-dimethylphenyl isocyanate (2.4 g, 16.1 mmol) generated W{N(2,6-Me-C₆H₃)}Cl₄ (4.0 g) as a dark red solid in 62% yield. Recrystallisation afforded orange crystals of **1.2** in an isolated yield of 70%. Anal. Calcd (found) (%) C 27.88 (28.00), H 3.32 (3.32), N 2.71 (2.80). ¹H NMR (*d*₆-benzene) δ (ppm): 6.78 (d, 2H, ArH_{meta}), 5.91 (dd, 1H, ArH_{para}), 4.43 (m, 4H, THF), 3.35 (s, 6H, Ar_{ortho}CH₃), 1.27 (m, 4H, THF). ¹³C{¹H} NMR (*d*₆-benzene) δ (ppm): 148.1 (Ar_{ipso}N), 145.6 (Ar_{ortho}CH₃),

133.8 (**Ar_{para}H**), 126.2 (**Ar_{meta}H**), 73.6 (**THF**), 25.4 (**THF**), 17.7 (**Ar_{ortho}CH₃**).

W{N(3,5-Me-C₆H₃)}Cl₄(THF) (1.3). W(O)Cl₄ (5.0 g, 14.6 mmol) and 3,5-dimethylphenyl isocyanate (2.4 g, 16.1 mmol) generated W{N(3,5-Me-C₆H₃)}Cl₄ (7.0 g) as a dark red solid in 84% yield. Recrystallisation afforded orange crystals of **1.3** in an isolated yield of 73%. Anal. Calcd (found) (%) C 27.88 (27.86), H 3.32 (3.35), N 2.71 (2.72). ¹H NMR (*d*₆-benzene) δ (ppm): 6.84 (s, 2H, **Ar_{ortho}H**), 5.85 (s, 1H, **Ar_{Hpara}**), 4.50 (m, 4H, **THF**), 1.60 (s, 6H, **Ar_{meta}CH₃**), 1.30 (m, 4H, **THF**). ¹³C{¹H} NMR (*d*₆-benzene) δ (ppm): 148.6 (**Ar_{ipso}N**), 137.1 (**Ar_{meta}CH₃**), 137.0 (**Ar_{para}H**), 129.6 (**Ar_{ortho}H**), 73.9 (**THF**), 25.5 (**THF**), 21.1 (**Ar_{meta}CH₃**).

W{N(2,4,6-Me-C₆H₂)}Cl₄(THF) (1.4). W(O)Cl₄ (10.6 g, 31.0 mmol) and 2,4,6-trimethylphenyl isocyanate (5.0 g, 31.0 mmol) yielded W{N(C₆H₂(2,4,6-Me))}Cl₄ (10.2 g) as a dark red solid in 72% yield. ¹H NMR (*d*₆-benzene) δ (ppm): 6.43 (s, 2H, **Ar_{Hmeta}**), 3.06 (s, 6H, **Ar_{ortho}CH₃**), 2.57 (s, 3H, **Ar_{para}CH₃**).

Dissolution in THF led to a dark green/brown solution and an orange solid after drying. Recrystallisation afforded orange crystals of **1.4**, isolated yield of 80%. Anal. Calcd (found) (%) C 29.41 (29.46), H 3.61 (3.78), N 2.64 (2.57). ¹H NMR (*d*₆-benzene) δ (ppm): 6.55 (s, 2H, **Ar_{Hmeta}**), 4.55 (m, 4H, **THF**), 3.39 (s, 6H, **Ar_{ortho}CH₃**), 2.6 (s, 3H, **Ar_{para}CH₃**), 1.27 (m, 4H, **THF**). ¹³C{¹H} NMR (*d*₆-benzene) δ (ppm): 146.4 (**Ar_{ipso}N**), 145.8 (**Ar_{ortho}CH₃**), 145.3 (**Ar_{para}CH₃**), 126.6 (**Ar_{meta}H**), 73.5 (**THF**), 25.4 (**THF**), 19.9 (**Ar_{para}CH₃**), 17.6 (**Ar_{ortho}CH₃**).

W{N(4-OMe-C₆H₄)}Cl₄(THF) (1.5). W(O)Cl₄ (10.0 g, 29.3 mmol) and 4-methoxyphenyl isocyanate (4.8 g, 32.2 mmol) yielded W{N(4-OMe-C₆H₄)}Cl₄ (10.2 g) as a dark blue solid in 88% yield. Dissolution in THF and drying afforded a dark red solid. Recrystallisation from pentane at -33 °C yielded dark red crystals of **1.5** in an isolated yield of 67%. Anal. Calcd (found) (%) C 27.33 (27.22), H 3.13 (3.02), N 2.90 (2.70). ¹H NMR (*d*₆-benzene) δ (ppm): 6.98 (d, 2H, **Ar_{Hortho}**), 6.41 (2, 2H, **Ar_{Hmeta}**), 4.51 (**THF**), 3.10 (**Ar_{para}OCH₃**), 1.29 (**THF**). ¹³C{¹H} NMR (*d*₆-benzene) δ (ppm): 164.8 (**Ar_{para}OCH₃**), 144.0 (**Ar_{ipso}N**), 134.3 (**Ar_{ortho}H**), 112.5 (**Ar_{meta}H**), 73.8 (**THF**), 56.0 (**Ar_{para}OCH₃**), 25.4 (**THF**).

W{N(2,6-F-C₆H₃)}Cl₄(THF) (1.6). W(O)Cl₄ (5.0 g, 14.6 mmol) and 2,6-difluorophenyl isocyanate (2.5 g, 16.1 mmol) yielded W{N(2,6-F-C₆H₃)}Cl₄ (6.1 g) as a dark red solid (79% yield). Dissolution in THF led to a dark green solution and a dark green solid after drying. Recrystallisation yielded dark green crystals of **1.6** in an isolated yield of 80%. Anal. Calcd (found) (%) C 22.89 (22.75), H 2.11 (2.12), N 2.67 (2.76). ¹H NMR (*d*₆-benzene) δ (ppm): 6.20 (t, 2H, **Ar_{Hmeta}**), 5.62 (m, 1H, **Ar_{Hpara}**), 4.45 (m, 4H, **THF**), 1.24 (m, 4H, **THF**). ¹³C{¹H} NMR (*d*₆-benzene) δ (ppm): 167.1 (**Ar_{ortho}F₂**), 164.5 (**Ar_{ipso}N**), 134.7 (**Ar_{para}H**), 110.0 (**Ar_{meta}H**), 74.3 (**THF**), 25.4 (**THF**). ¹⁹F{¹H} NMR (*d*₆-benzene) δ (ppm): -111.04.

W{N(3,5-CF₃-C₆H₃)}Cl₄(THF) (1.7). W(O)Cl₄ (5.0 g, 14.6 mmol) and 3,5-bis(trifluoromethyl)phenyl isocyanate (4.1 g, 16.1 mmol) yielded W{N(3,5-CF₃-C₆H₃)}Cl₄ (5.35 g) as a dark green solid in 65% yield. W{N(3,5-CF₃-C₆H₃)}Cl₄ (100 mg) was dissolved in THF and dried. Dichromic yellow/blue crystals of **1.7** were grown from pentane at -33 °C in a crystalline yield of

25%. Anal. Calcd (found) (%) C 23.07 (23.21), H 1.77 (1.79), N 2.24 (2.33). ¹H NMR (*d*₆-benzene) δ (ppm): 7.43 (s, 2H, **Ar_{Hortho}**), 6.96 (s, 1H, **Ar_{Hpara}**), 4.39 (m, 4H, **THF**), 1.24 (m, 4H, **THF**). ¹³C{¹H} NMR (*d*₆-benzene) δ (ppm): 150.0 (**Ar_{ipso}N**), 130.6 (**Ar_{para}H**), 126.0 (**Ar_{ortho}H**), 124.4 (**Ar_{meta}(CF₃)₂**), 121.6 (**Ar_{meta}(CF₃)₂**), 74.6 (**THF**), 25.4 (**THF**). ¹⁹F{¹H} NMR (*d*₆-benzene) δ (ppm): -63.15.

General Procedure for the Synthesis of W(NR)Me₃Cl Complexes. The following syntheses were based on a literature procedure.¹² W(NR)Cl₄(THF) (0.5-1 g) was added to a Rotaflow ampoule and dissolved in benzene (20 mL). Excess TMA was added (~1.2 eq.) and the mixture stirred for 1 hour. An immediate colour change was observed with mixing in all cases. The product was extracted from hexane and purified by fractional crystallisation at -33 °C. Crystals suitable for single crystal X-ray diffraction studies grew once all the residual aluminium compounds had been removed.

W{N(C₆H₅)}Me₃Cl (2.1). Pale yellow crystalline solid in 20% yield. Anal. Calcd (found) (%) C 30.41 (30.54), H 3.97 (4.08), N 3.94 (3.97). ¹H NMR (*d*₆-benzene) δ (ppm): 7.01 (m, 2H, **Ar_{Hmeta}**), 6.99 (d, 2H, **Ar_{Hortho}**), 6.88 (m, 2H, **Ar_{Hpara}**), 1.29 (s, 9H, W(CH₃)₃, ²J_{W-H} = 6.84 Hz). ¹³C{¹H} NMR (*d*₆-benzene) δ (ppm): 152.1 (**Ar_{ipso}N**), 128.8 (**Ar_{meta}H**), 127.9 (**Ar_{para}H**), 127.6 (**Ar_{ortho}H**), 53.6 (W(CH₃)₃, ¹J_{W-C} = 299.0 Hz).

W{N(2,6-Me-C₆H₃)}Me₃Cl (2.2). Orange crystalline solid in 42% yield. Anal. Calcd (found) (%) C 34.45 (34.53), H 4.73 (4.82), N 3.65 (3.66). ¹H NMR (*d*₆-benzene) δ (ppm): 6.83 (d, 2H, **Ar_{Hmeta}**), 6.74 (t, 1H, **Ar_{Hpara}**), 2.21 (s, 6H, **Ar_{ortho}CH₃**), 1.34 (s, 9H, W(CH₃)₃, ²J_{W-H} = 7.18 Hz). ¹³C{¹H} NMR (*d*₆-benzene) δ (ppm): 150.4 (**Ar_{ipso}N**), 139.6 (**Ar_{ortho}CH₃**), 127.9 (**Ar_{meta}H**), 127.4 (**Ar_{para}H**), 56.1 (W(CH₃)₃, ¹J_{W-C} = 302.2 Hz), 19.4 (**Ar_{ortho}CH₃**).

W{N(3,5-Me-C₆H₃)}Me₃Cl (2.3). Yellow crystalline solid in 61% yield. Anal. Calcd (found) (%) C 34.45 (34.38) H 4.73 (4.85) N 3.65 (3.60). ¹H NMR (*d*₆-benzene) δ (ppm): 6.85 (s, 2H, **Ar_{ortho}H**), 6.58 (s, 1H, **Ar_{para}H**), 1.99 (s, 6H, **Ar_{meta}CH₃**), 1.34 (s, 9H, W(CH₃)₃, ²J_{W-H} = 7.20 Hz). ¹³C{¹H} NMR (*d*₆-benzene) δ (ppm): 152.3 (**Ar_{ipso}N**), 138.5 (**Ar_{meta}CH₃**), 130.4 (**Ar_{para}H**), 125.3 (**Ar_{ortho}H**), 53.6 (W(CH₃)₃, ¹J_{W-C} = 276.4 Hz), 21.1 (**Ar_{meta}CH₃**).

W{N(4-OMe-C₆H₄)}Me₃Cl (2.5). Yellow crystalline solid in 23% yield. Anal. Calcd (found) (%) C 31.15 (30.88), H 4.18 (4.29), N 3.63 (3.65). ¹H NMR (*d*₆-benzene) δ (ppm): 6.99 (d, 2H, **Ar_{Hortho}**), 6.61 (d, 2H, **Ar_{Hmeta}**), 3.23 (s, 3H, **Ar_{para}OCH₃**), 1.30 (s, 9H, W(CH₃)₃, ²J_{W-H} = 6.88 Hz). ¹³C{¹H} NMR (*d*₆-benzene) δ (ppm): 160.0 (**Ar_{para}OCH₃**), 144.0 (**Ar_{ipso}N**), 129.1 (**Ar_{ortho}H**), 114.1 (**Ar_{meta}H**), 55.1 (**Ar_{para}OCH₃**), 53.5 (W(CH₃)₃, ¹J_{W-C} = 300.8 Hz).

W{N(2,6-F-C₆H₃)}Me₃Cl (2.6). Orange crystalline solid in 35% yield. Anal. Calcd (found) (%) C 27.61 (27.49), H 3.09 (2.98), N 3.58 (3.59). ¹H NMR (*d*₆-benzene) δ (ppm): 6.36 (m, 2H, **Ar_{Hmeta}**), 6.30 (m, 1H, **Ar_{Hpara}**), 1.45 (s, 9H, W(CH₃)₃, ²J_{W-H} = 7.44 Hz). ¹³C{¹H} NMR (*d*₆-benzene) δ (ppm): 163.9 (**Ar_{ipso}N**), 161.3 (**Ar_{ortho}F₂**), 127.6 (**Ar_{para}H**), 111.5 (**Ar_{meta}H**), 54.4 (W(CH₃)₃, ¹J_{W-C} = 295.6 Hz). ¹⁹F{¹H} NMR (*d*₆-benzene) δ (ppm): -117.6. ¹³C-{¹H} CPMAS {¹⁹F} decoupled solid-state NMR δ (ppm): 162.2 (**Ar_{ortho}F**), 160.8 (**Ar_{ipso}N**), 129.1 (**Ar_{para}H**), 109.8

(Ar_{meta}H), 59.0 (W(CH₃)₂), 55.0 (W(CH₃)). ¹⁹F{¹H} DPMAS solid-state NMR δ (ppm): −116.3.

Synthesis of W{N(2,6-F-C₆H₃)}{¹³CH₃}₃Cl (2.6*). Following the same procedure detailed above, **1.6** (50 mg, 0.10 mmol) was reacted with Al(¹³CH₃)₃ (1.1 eq) in *d*₆-benzene in a Young's NMR tube. Removal of the solvent and recrystallisation from hexane yielded **2.6*** (10 mg) as a yellow solid in 27% yield. The solution NMR spectroscopic data matched that of **2.6**.

General Procedure for the Immobilisation of Complexes on sMAO. A W:Al ratio of 1:150 was used unless otherwise stated. sMAO (100 mg, 39.7% wt Al, 1.47 mmol) and W(NR)Cl₄(THF) or **2.6*** were mixed in 50 mL of toluene, and swirled at regular intervals at room temperature for 1 h. A colour change from a white solid and coloured solution to a pale coloured solid with a colourless solution was observed indicating that all of the tungsten complex had been immobilised. The solid was left to settle and the supernatant was filtered off and dried in vacuo in near quantitative yield. An NMR scale reaction of sMAO (20 mg, 0.29 mmol) and **1.3** (1 mg, 1.94 μmol) in *d*₆-benzene (0.5 mL), showed the complete disappearance of resonances attributed to **1.3** with only toluene present from sMAO synthesis and a small amount of methane observed in the ¹H NMR spectrum.

sMAO. White solid. 39.7 wt% Al. ¹³C-{¹H} CP-MAS solid-state NMR δ (ppm): 177 (PhCO₂), 129 (PhCO₂), −7 (strong, Al(CH₃)).

sMAO-1.1. Pale straw solid.

sMAO-1.2. Pale yellow solid.

sMAO-1.3. Pale yellow solid.

sMAO-1.4. Pale yellow solid.

sMAO-1.5. Pale yellow solid. ¹³C{¹H} CP-MAS solid-state NMR δ (ppm): 177 (PhCO₂), 136 (Ar), 131 (PhCO₂), 128 (Ar), 114 (Ar, v. weak), 73 (THF), 62 (OCH₃, weak), 54 (W(CH₃)₃, v. weak), 25 (THF), −8 (strong, Al(CH₃)).

sMAO-1.6. Yellow solid. ¹³C{¹H} CP-MAS solid-state NMR δ (ppm): 130 (PhCO₂), 123 (ArF), 105 (Ar, v.weak), 67 (broad, THF, W(CH₃)₃), 18 (THF), −7 (strong, Al(CH₃)). ¹⁹F{¹H} MAS solid-state NMR δ (ppm): −123.

sMAO-1.7. Pale brown solid. ¹³C{¹H} CP-MAS solid-state NMR δ (ppm): 129 (PhCO₂), 121 (Ar), −14 (strong, Al(CH₃)). Low S:N ratio. ¹⁹F{¹H} MAS solid-state NMR δ (ppm): −141 (broad, Al-F), −69 (CF₃ supported complex).

sMAO-2.6*. Yellow solid. ¹³C{¹H} CP-MAS solid-state NMR δ (ppm): 177 (PhCO₂), 155 (ArF), 129 (PhCO₂), 125 (Ar), 105 (Ar), 85 (Ar), 56, 45 (W(CH₃)₃, broad), −7 (strong, Al(CH₃)). ¹⁹F{¹H} MAS solid-state NMR δ (ppm): −123.

The aluminium and tungsten content of samples of sMAO-1.4, sMAO-1.5 and sMAO-1.7 were analysed by ICP-MS after digestion in refluxing HNO₃ and subsequent dilutions with distilled water (Table S3). Results show a much lower complex loading than was evidenced by solution NMR spectroscopy (61.4, 53.5 and 61.2% respectively). This may be due to incomplete digestion of the tungsten component, as tungsten oxide species that can form in acidic media are extremely difficult to breakdown, requiring aggressive hydrofluoric acid treatment.^{60,61} Due to the highly exothermic reaction between sMAO and acidic media this digestion method was not attempted.

General Procedure for Testing the Ethylene Oligomerisation Activity of the Solid Catalysts. sMAO supported catalyst (5 mg, 0.47 μmol of W) was added to a Young's NMR tube. Deuterated solvent (500 μL) and mesitylene (2.8 μL, 20.1 μmol) were added *via* microlitre syringe. The contents were freeze-pump-thaw degassed three times and 1 bar of ethylene introduced. The reaction was heated in an oil bath at a specified temperature and a ¹H NMR spectrum taken periodically. TONs were calculated by integration of product peaks relative to the mesitylene standard; 1-butene (1.90 ppm), *trans*-2-butene (1.50 ppm), *cis*-2-butene (1.57 ppm), propylene (1.54 ppm). In the cases of *d*₈-THF, *d*₂-DCM and *d*₁₈-octane the solvent resonances obscured the peak at 1.9 ppm and hence the resonance at 0.98 or 5.4 ppm were integrated.

Reactivity towards 1-hexene and 1-octene. sMAO-1.6 (5 mg, 0.47 μmol of W) was added to a Young's NMR tube and *d*₆-benzene (500 μL) and 1-hexene or 1-octene (40 μmol) added *via* microliter syringe. The tube was heated at 75 °C and ¹H NMR spectra recorded periodically. Isomerisation of the olefin was observed in both cases to yield the *cis*- and *trans*-2-alkenes.

Acknowledgements

The authors would like to thank Dr. Nicholas H. Rees for solid-state NMR spectroscopy, Dr. Alexander F. R. Kilpatrick for synthesis of the polymethylaluminoxane support and assistance with ICP-MS sample preparation, Chemical Crystallography (University of Oxford) for use of the diffractometers, SCG Chemicals Co. Ltd, Thailand for an innovation fund grant (C.M.R.W.) and funding (Z.R.T. and J.-C.B.), the Engineering and Physical Sciences Research Council (U.K.) (EP/L50503/1) for funding (C.M.R.W.) and Trinity College Oxford for a Junior Research Fellowship (Z.R.T.).

Notes and references

1. S. F. Pedersen and R. R. Schrock, *J. Am. Chem. Soc.*, 1982, **104**, 7483–7491.
2. R. R. Schrock and A. H. Hoveyda, *Angew. Chem. Int. Ed.*, 2003, **42**, 4592–4633.
3. R. R. Schrock, *Chem. Rev.*, 2002, **102**, 145–180.
4. D. Astruc, *New J. Chem.*, 2005, **29**, 42–56.
5. J. C. Axtell, R. R. Schrock, P. Müller, S. J. Smith, and A. H. Hoveyda, *Organometallics*, 2014, **33**, 5342–5348.
6. H. R. Menapace, N. A. Maly, J. L. Wang, and L. G. Wideman, *J. Org. Chem.*, 1975, **40**, 2983–2985.
7. M. J. Hanton, L. Daubney, T. Lebl, S. Polas, D. M. Smith, and A. Willemse, *Dalton Trans.*, 2010, **39**, 7025–7037.
8. W. R. H. Wright, A. S. Batsanov, J. A. K. Howard, R. P. Tooze, M. J. Hanton, and P. W. Dyer, *Dalton Trans.*, 2010, **39**, 7038–7045.
9. H. Olivier and P. Laurent-Gérot, *J. Mol. Catal. A Chem.*, 1999, **148**, 43–48.
10. E. Kaji and E. Yoshioka, *Solid polymethylaluminoxane*

- composition and process for manufacturing same*, 2010, WO2010055652.
11. A. F. R. Kilpatrick, J.-C. Buffet, P. Nørby, N. H. Rees, N. P. Funnell, S. Sripothongnak, and D. O'Hare, *Chem. Mater.*, 2016, **28**, 7444–7450.
 12. C. M. R. Wright, Z. R. Turner, J.-C. Buffet, and D. O'Hare, *Chem. Commun.*, 2016, **52**, 2850–2853.
 13. T. L. Lohr and T. J. Marks, *Nat. Chem.*, 2015, **7**, 477–482.
 14. G. Lappin, *Alpha olefins applications handbook*, CRC Press, 1989.
 15. T. Agapie, *Coord. Chem. Rev.*, 2011, **255**, 861–880.
 16. V. Mougel, C. B. Santiago, P. A. Zhizhko, E. N. Bess, J. Varga, G. Frater, M. S. Sigman, and C. Copéret, *J. Am. Chem. Soc.*, 2015, **137**, 6699–6704.
 17. D. C. Bradley, M. B. Hursthouse, K. M. A. Malik, A. J. Nielson, and R. L. Short, *J. Chem. Soc. Dalton Trans.*, 1983, 2651–2656.
 18. L. K. Johnson, R. H. Grubbs, and J. W. Ziller, *J. Am. Chem. Soc.*, 1993, **115**, 8130–8145.
 19. D. C. Bradley, S. R. Hodge, J. D. Runnacles, M. Hughes, J. Mason, and R. L. Richards, *J. Chem. Soc. Dalton Trans.*, 1992, 1663–1668.
 20. R. R. Schrock, R. T. DePue, J. Feldman, K. B. Yap, D. C. Yang, W. M. Davis, L. Park, M. DiMare, M. Schofield, J. Anhaus, E. Walborsky, E. Evitt, C. Krüger, and P. Betz, *Organometallics*, 1990, **9**, 2262–2275.
 21. D. C. Bradley, R. J. Errington, M. B. Hursthouse, R. L. Short, B. R. Ashcroft, G. R. Clark, A. J. Nielson, and C. E. F. Rickard, *J. Chem. Soc. Dalton Trans.*, 1987, 2067–2075.
 22. J. C. Duhacek, T. A. Siddiquee, D. W. Bennett, and D. C. Duncan, *J. Chem. Crystallogr.*, 2008, **38**, 431–435.
 23. T. S. Pilyugina, R. R. Schrock, A. S. Hock, and P. Müller, *Organometallics*, 2005, **24**, 1929–1937.
 24. F. G. Bordwell, X. M. Zhang, and J. P. Cheng, *J. Org. Chem.*, 1993, **58**, 6410–6416.
 25. F. G. Bordwell and D. J. Algrim, *J. Am. Chem. Soc.*, 1988, **110**, 2964–2968.
 26. I. A. Guzei and M. Wendt, *Dalton Trans.*, 2006, 3991–3999.
 27. E. Wiberg and N. Wiberg, *Inorganic Chemistry*, Academic Press, 2001.
 28. W. P. Griffith, A. J. Nielson, and M. J. Taylor, *J. Chem. Soc. Dalton Trans.*, 1988, 647–649.
 29. ChemAxon, <http://www.chemicalize.org/>.
 30. V. C. Gibson, C. Redshaw, G. L. P. Walker, J. A. K. Howard, V. J. Hoy, J. M. Cole, L. G. Kuzmina, and D. S. De Silva, *J. Chem. Soc. Dalton Trans.*, 1999, 161–166.
 31. D. A. X. Fraser, Z. R. Turner, J.-C. Buffet, and D. O'Hare, *Organometallics*, 2016, **35**, 2664–2674.
 32. T. A. Q. Arnold, Z. R. Turner, J.-C. Buffet, and D. O'Hare, *J. Organomet. Chem.*, 2016, **822**, 85–90.
 33. J.-M. Basset, R. Psaro, D. Roberto, and R. Ugo, Eds., *Modern Surface Organometallic Chemistry*, Wiley-VCH Verlag GmbH & Co. KGaA, Weinheim, Germany, 2009.
 34. F. Ghiotto, C. Pateraki, J. Tanskanen, J. R. Severn, N. Luehmann, A. Kusmin, J. Stellbrink, M. Linnolahti, and M. Bochmann, *Organometallics*, 2013, **32**, 3354–3362.
 35. P. J. Chupas and C. P. Grey, *J. Catal.*, 2004, **224**, 69–79.
 36. J. Terao, M. Nakamura, and N. Kambe, *Chem. Commun.*, 2009, 6011–6013.
 37. A. Kermagoret, R. N. Kerber, M. P. Conley, E. Callens, P. Florian, D. Massiot, F. Delbecq, X. Rozanska, C. Copéret, and P. Sautet, *J. Catal.*, 2014, **313**, 46–54.
 38. C. Copéret, A. Comas-Vives, M. P. Conley, D. P. Estes, A. Fedorov, V. Mougel, H. Nagae, F. Núñez-Zarur, and P. A. Zhizhko, *Chem. Rev.*, 2016, **116**, 323–421.
 39. W. Kaminsky, S. Lenk, V. Scholz, H. W. Roesky, and A. Herzog, *Macromolecules*, 1997, **30**, 7647–7650.
 40. Y. Chen, C. L. Stern, and T. J. Marks, *J. Am. Chem. Soc.*, 1997, **119**, 2582–2583.
 41. Y. X. Chen, M. V. Metz, L. Li, C. L. Stern, and T. J. Marks, *J. Am. Chem. Soc.*, 1998, **120**, 6287–6305.
 42. P. Cossee, *J. Catal.*, 1964, **3**, 80–88.
 43. R. Schrock, S. McLain, and J. Sancho, *Pure Appl. Chem.*, 1980, **52**, 729–732.
 44. S. J. McLain and R. R. Schrock, *J. Am. Chem. Soc.*, 1978, **100**, 1315–1317.
 45. J. D. Fellmann, G. A. Rupprecht, and R. R. Schrock, *J. Am. Chem. Soc.*, 1979, **101**, 5099–5101.
 46. S. Tobisch, *Organometallics*, 2007, **26**, 6529–6532.
 47. C. Reichardt and T. Welton, *Solvents and Solvent Effects in Organic Chemistry*, Wiley-VCH Verlag GmbH & Co. KGaA, Weinheim, Germany, 2010, vol. 16.
 48. F. Cataldo, *Eur. Chem. Bull.*, 2015, **4**, 92–97.
 49. P. R. Elowe, C. McCann, P. G. Pringle, S. K. Spitzmesser, and J. E. Bercaw, *Organometallics*, 2006, **25**, 5255–5260.
 50. J. Cosier and A. M. Glazer, *J. Appl. Crystallogr.*, 1986, **19**, 105–107.
 51. CrysAlisPro, Oxford Diffraction/Agilent Technologies UK LTD, Yarnton, England.
 52. Z. Otwinowski and W. Minor, in *Macromolecular Crystallography Part A*, ed. J. B. T.-M. in E. Charles W. Carter, Academic Press, 1997, vol. Volume 276, pp. 307–326.
 53. R. H. Blessing, *Acta Crystallogr. Sect. A*, 1995, **51**, 33–38.
 54. A. Altomare, G. Cascarano, C. Giacovazzo, and A. Guagliardi, *J. Appl. Crystallogr.*, 1993, **26**, 343–350.
 55. L. Palatinus and G. Chapuis, *J. Appl. Crystallogr.*, 2007, **40**, 786–790.
 56. L. J. Farrugia, *J. Appl. Crystallogr.*, 2012, **45**, 849–854.
 57. L. J. Farrugia, *J. Appl. Crystallogr.*, 1999, **32**, 837–838.
 58. V. C. Gibson, T. P. Kee, and A. Shaw, *Polyhedron*, 1988, **7**, 579–580.
 59. K. P. Bryliakov, E. P. Talsi, and M. Bochmann, *Organometallics*, 2004, **23**, 149–152.
 60. A. J. Bednar, W. T. Jones, M. A. Chappell, D. R. Johnson, and D. B. Ringelberg, *Talanta*, 2010, **80**, 1257–1263.
 61. C. E. McGinnis, J. C. Jain, and C. R. Neal, *Geostandards Newsletter*, 1992, **21**, 289–305.